Numerical Simulation on the Shielding Efficiency of Magnetic Shielding Enclosures in the ITER Applications

Yong Kou[1], Ke Jin[1] and Xiaojing Zheng[1,2]

Abstract: Magnetic shielding needs to be employed to ensure proper operation of some electronic equipment which are sensitive to external magnetic interference, such as cryogenic valves located inside the ITER feeder cubicles. This paper is concerned with the shielding efficiency of the magnetic shielding enclosures. A 3-D theoretical model for Fe-Ni alloy magnetic shielding enclosures based on finite element method (FEM) is obtained with the nonlinear law of magnetization. The influence of shielding materials, enclosure configurations, single or multi- layer designs, and apertures on the shielding efficiency is investigated. It is shown that the proposed model can predict the shielding efficiency of shielding devices well with nonlinear magnetize relation, and some recommendations for an optimized magnetic shield design in the ITER feeder cubicles are given.

Keywords: Magnetic shielding, Nonlinear law of magnetization, Apertures, Multilayer.

1   Introduction

The ambient magnetic field around ITER feeder cubicles will cause considerable disturbance to the operation and accuracy of sensitive electrical and electronic equipment located inside the cubicles such as cryogenic valves. Since the admissible level of magnetic fields for these valves should be less than 5mT, magnetic shielding needs to be applied to ensure proper operation of these equipment. Fe-Ni alloys have an immeasurable applied prospect in the field of magnetic shielding. However, the nonlinear magnetization behavior inherent to these alloys would have an influence on the shielding efficiency. Moreover, the thicknesses of the shielding enclosures are limited because the cryogenic valves are numerous and densely

---

[1] Key Laboratory of Mechanics on Environment and Disaster in Western China, The Ministry of Education of China, and Department of Mechanics and Engineering Sciences, School of Civil Engineering and Mechanics, Lanzhou University, Lanzhou, Gansu 730000, P.R. China

[2] Author to whom correspondence should be addressed; electronic mail: xjzheng@lzu.edu.cn

arranged. In that case, sufficient magnetic shielding effect can be achieved with multilayer enclosure [Bottauscio, Chiampi and Manzin (2004)] if single layer enclosure cannot meet the shielding requirement under the thickness limits. The effects of the physics and geometric parameters for each layer and the insulative layer between two adjacent layers on the shielding efficiency must be considered. Furthermore, there are some unavoidable apertures located on walls of the shielding enclosure, such as the apertures for monitors and feeder connection. The shielding is affected significantly by these apertures. It is therefore important to characterize the shielding efficiency of enclosures with various apertures.

The concept of magnetic shielding goes back to John Baptist Porta in 1589. However, it is not until three centuries later that Rucker [Rucker (1894)] derives the formulae for the transverse shielding factor of infinitely long multilayer concentric shields. Sumner et al [Sumner, Pendlebury and Smith (1987)] later presents a solution for shielding factor of a finitely long multilayer cylinder shield. Although these solutions can give some qualitative results on the magnetic shielding, the shielding factor they derived is independent of the ambient magnetic field. Furthermore, the distributions of the magnetic field intensity inside the shields can not be captured by their works. Hoburg [Hoburg (1996)] maintains a set of formulae for multilayer shields, but his methodology mainly focuses on the shields with isopachous layers and linear magnetized materials, which may be inaccurate in case of a highly nonlinear material and a strongly non-uniform field distribution in the shield [Koroglu, Sergeant and Umurkan (2010)]. Despite the fact that the analytical method is convenience, it is only valid for simple shield geometry and limited by a lot of assumptions. For some complex enclosure configurations, it is difficult to obtain a set of closed and analytical expressions. Thus the use of numerical methods is indispensable. There exist many works carried out by numerical methods. Omura et al [Omura, Kotani, Yasu and Itoh (2006)] calculate the distribution of the magnetic field within a cylinder shield by use of the finite element method (FEM). Wulf et al [Wulf, Wouters, Sergeantc, Dupré, Hoferlin, Jacobs and Harlet (2007)] study the electromagnetic shielding of high-voltage (HV) cables by FEM numerical simulations and experiments. In their studies, two shield configurations, i.e. open and closed shields, have been considered. Umurkan et al [Koroglu, Umurkan, Kilic and Attar (2009); Umurkan, Koroglu and Kilic (2010)] apply a neural network method to estimate multilayered magnetic shielding performances. The primary advantage of the neural network method is fast and easy implementation. However, it has the disadvantage that an initial "training" should be carried out based on an amount of measurements, and the shield geometry and material properties are not taken into account. Therefore, the neural network method is still rather complicated in some complex shield configurations, such as shielding enclosure with apertures. There

exist many works considering the influence of apertures on shielding efficiency. Shen et al develop a hybrid numerical technique combining the finite-difference (FD) method and the method of moments (MoM) to predict the shielding efficiency of rectangular enclosures with single rectangular aperture [Feng and Shen (2005)], cylinderical enclosures with a ring aperture [Shen (2006)] and cylindrical enclosures with a rectangular aperture [Shen and Zheng (2008)]. Yenikaya and Akman [Yenikaya and Akman (2009)] present a hybrid technique which combines MoM and FEM to predict shielding efficiency for a dielectric slab loaded enclosure with single aperture. Kumar and Venkatesh [Kumar and Venkatesh (2009)] discuss the influence of aperture shape on the shielding efficiency by TLM method. However, all of these works focus on the shields with single apertrue and the shielding effectiveness at one point (at the center of the shield generally), whereas the study of the distribution of shielding effectiveness inside the shields is more substantial for engineering applications. Moreover, none of the above models take into account the nonlinear law of magnetization. Koroglu et al [Koroglu, Sergeant and Umurkan (2010)] compare analytical, finite element and neural network methods with nonlinear magnetization behavior in studying magnetic shielding, but the FEM adopted is 2-dimensional model, which may be inaccurate in practical applications.

In this paper, a 3-D theoretical model for Fe-Ni alloy magnetic shielding enclosures based on FEM with the nonlinear law of magnetization is developed. With this model, a step by step analysis of possible magnetic shielding design is presented. The influence of parameters for shielding materials and enclosure configurations on the shielding efficiency is shown firstly. And an investigation of the effects of the number, area and location of apertures on shielding is given next. Furthermore, single or multi- layer designs for shields are also discussed and some recommendations for an optimized magnetic shield design in the ITER feeder cubicles are given. This paper is organized as follows. Basic equations for magnetic shielding enclosure are given in Section 2 with introducing the linear and nonlinear law of magnetization. FEM numerical approaches as well as experimental measurements are presented in Section 3. Finally, Section 4 concludes the work investigated in the paper.

2   Basic equations

The problem considered in the paper is shown in Fig. 1. A rectangular enclosure of dimension a×b×c with rectangular or circular apertures (Aperture 1, Aperture 2, ..., Aperture N) in various size is constructed in Fig. 1(a). The transverse section plan of the multi-layer enclosure is shown in Fig. 1(b), in which t_1, t_2, ..., t_n are respectively the thickness of each layer.

The electromagnetic field distributions inside and outside the enclosure can be ob-
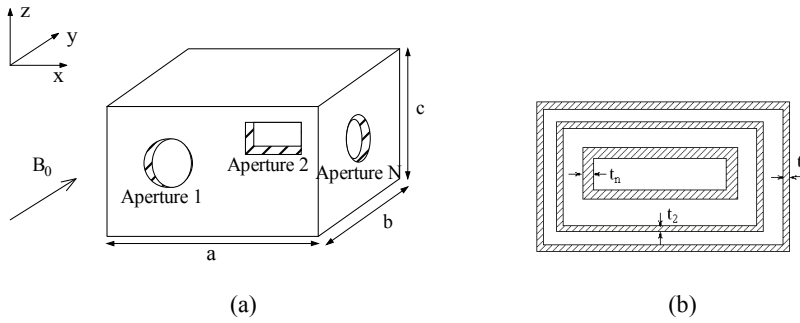
Figure 1: The model of a rectangular shielding enclosure with apertures under external magnetic field $\mathbf{B}_0$.

tained from Maxwell equations,

$$\nabla \cdot \mathbf{D} = q_e, \tag{1}$$

$$\nabla \times \mathbf{E} + \frac{\partial \mathbf{B}}{\partial t} = \mathbf{0}, \tag{2}$$

$$\nabla \cdot \mathbf{B} = 0, \tag{3}$$

$$\nabla \times \mathbf{H} = \mathbf{J}_e + \frac{\partial \mathbf{D}}{\partial t}, \tag{4}$$

where $\mathbf{B}$ and $\mathbf{H}$ are magnetic induction and magnetic field intensity respectively, $\mathbf{E}$ and $\mathbf{D}$ are respectively electric field intensity and electric displacement, q_e and $\mathbf{J}_e$ are respectively the free charge density and the free current density.

Let $\mathbf{n}$ represent a unit vector normal to the surface S of the medium, then the boundary conditions for electromagnetic field are

$$\mathbf{n}^+ \cdot [\![\mathbf{D}]\!] = q_S, \tag{5}$$

$$\mathbf{n}^+ \times [\![\mathbf{E}]\!] = \mathbf{0}, \tag{6}$$

$$\mathbf{n}^+ \cdot [\![\mathbf{B}]\!] = 0, \tag{7}$$

$$\mathbf{n}^+ \times [\![\mathbf{H}]\!] = \mathbf{J}_S. \tag{8}$$

in which q_s and $\mathbf{J}_s$ are respectively the surface charge density and the surface current density. $[\![A]\!] = A^+ - A^-$, for an interface between the material and the air, A^+ and A^- are the magnetic field quantities in the material and the air (or vacuum) respectively.

Usually, the values of ambient magnetic field around the electronic equipment located inside the ITER feeder cubicles are ranging from 1mT to 100mT. Thus, Fe-Ni alloys which have good shielding performance in the low field are chosen as shielding materials in this work. For simplicity, the assumption of homogeneous and isotropic magnetization law is adopted, which can be expressed as

$$\mathbf{B} = \mu_0 \mu_r(\mathbf{H})\mathbf{H}, \tag{9}$$

where, μ_0 is the permeability in vacuum, $\mu_r(\mathbf{H})$ is the relative permeability of Fe-Ni alloy materials which can be approximated by the following formulae

Linear dependence. If the linear law of magnetization is considered, $\mu_r(\mathbf{H})$ is a constant which will not be changed by the applied magnetic field.

$$\mu_r(\mathbf{H}) = \mu_r, \tag{10}$$

Nonlinear dependence. Experimental investigations show that the magnetic permeability becomes nonlinear (see Fig. 2). The relative permeability decreases as the magnetic field increases, thus, the Fröhlich form [Jiles (1991)] is used.

$$B(H) = H/(\alpha_1/\mu_0 + \alpha_2 H) + \mu_0 H, \tag{11}$$

and the relative permeability can be written as

$$\mu_r(H) = 1/(\alpha_1 + \alpha_2 \mu_0 H) + 1, \tag{12}$$

where, α_1 and α_2 are coefficients which can be determined from experiments.

3 Quantitative discussions

3.1 Numerical approach

For stationary magnetic fields, the conduction current on and in the magnetizable medium can be neglected. Thus, we can introduce a scalar potential function

$$\mathbf{H} = -\nabla \varphi, \tag{13}$$

After taking a closed surface Γ_0 far away from the medium, we can express the magnetic energy functional for the system

$$\Pi\{\varphi, \mathbf{u}\} = \int_{\Omega^+(\mathbf{u})} \left(\int_0^{H^+} B(H^+)dH^+ \right) dv + \frac{1}{2} \int_{\Omega^-(\mathbf{u})} \mu_0(\nabla\varphi^-)^2 dv + \int_{\Gamma_0} \mathbf{n}_0 \cdot \mathbf{B}_0 \varphi^- ds, \tag{14}$$

Having considered the arbitrariness and independence of $\delta\varphi$, one can easily get, from $\delta_\Phi\Pi\{\varphi\}=0$, all fundamental equations for magnetic fields inside and outside the enclosure.

Now, we will numerically analyze the magnetic field distribution in regions $\Omega^+(\mathbf{u})$ and $\Omega^-(\mathbf{u})$ based on finite element method. Having discretized $\Omega^+(\mathbf{u})$ and $\Omega^-(\mathbf{u})$ into several small elements and introduced shape function $\mathbf{N}^{em}$ to these elements, the unknown scalar potential can be defined with $\mathbf{N}^{em}$

$$\varphi(x,y,z) = [\mathbf{N}^{em}]_e[\Phi]_e, \tag{15}$$

in which $[\mathbf{N}^{em}]_e = [N_1^{em}, N_2^{em}, N_3^{em}, \cdots, N_M^{em}]$, $[\Phi]_e = [\phi_1, \phi_2, \phi_3, \cdots, \phi_M]^T$, M is the total node number of each element. Substituting Eq. (15) into Eq. (13), the magnetic field intensity on the nodes can be written as

$$H_x = -\frac{\partial\phi}{\partial x} = -[\frac{\partial\mathbf{N}^{em}}{\partial x}]_e[\Phi]_e, \tag{16}$$

$$H_y = -\frac{\partial\phi}{\partial y} = -[\frac{\partial\mathbf{N}^{em}}{\partial y}]_e[\Phi]_e, \tag{17}$$

$$H_z = -\frac{\partial\phi}{\partial z} = -[\frac{\partial\mathbf{N}^{em}}{\partial z}]_e[\Phi]_e, \tag{18}$$

From Eq. (14), the algebraic equation of magnetic scalar potential of the nodes for each element may now expressed as

$$[\mathbf{K}^{em}]_e[\Phi]_e = [\mathbf{P}]_e, \tag{19}$$

where

$$[\mathbf{K}^{em}]_e = \begin{cases} \int_{\Omega_e} \mu_0\mu_r[\nabla\mathbf{N}^{em}]_e^T[\nabla\mathbf{N}^{em}]_e dv, & \Omega_e \in \Omega^+(\mathbf{u}) \\ \int_{\Omega_e} \mu_0[\nabla\mathbf{N}^{em}]_e^T[\nabla\mathbf{N}^{em}]_e dv, & \Omega_e \in \Omega^-(\mathbf{u}) \end{cases}, \tag{20}$$

$$[\mathbf{P}]_e = \begin{cases} -\int_{\Gamma_e} \mathbf{n}_0 \cdot \mathbf{B}_0[\mathbf{N}^{em}]_e^T dS, & \Gamma_e \in \Gamma_0 \\ \mathbf{0}, & \Gamma_e \notin \Gamma_0 \end{cases}, \tag{21}$$

Assembling the element magnetic stiffness matrices $[\mathbf{K}^{em}]_e$ of all elements, we can write the global algebraic equation for the magnetic field

$$[\mathbf{K}^{em}][\Phi] = [\mathbf{P}], \tag{22}$$

where $[\Phi]$ is a column matrix of the unknown magnetic potential at all nodes, $[\mathbf{K}^{em}]$ is the global magnetic stiffness matrix and $[\mathbf{P}]$ is the matrix related to the applied magnetic field on Γ_0.

3.2   *Experimental measurement*

Fe-Ni alloy 1J79 is used in the experiments, and the rectangular enclosure is 223mm length, 116mm width and 3mm thickness. The maximum relative permeability is 40000 and the saturated magnetization is 0.65T. The experiment arrangement is composed of a high magnetization facility, which can provide a 2.4T cylindrical (100mm dia.) symmetrical magnet field at 100mm magnetic polar distance and the measurement precision is 0.001T. The magnetic field intensity measured by a Hall probe and gathered by a Guess meter. In this experiment, the magnetization relation of Fe-Ni alloy (see Fig. 2) and the shielding efficiency of the enclosure under 10mT-50mT external magnetic field (see Tab. 1) are measured. For the Fe-Ni alloy 1J79 used in this work, when the coefficients in the Eq. (6) chosen as $\alpha_1 = -3.0 \times 10^{-5}$, $\alpha_2 = 0.26$, the magnetization law has a good fit with the experimental data (see Fig. 2).
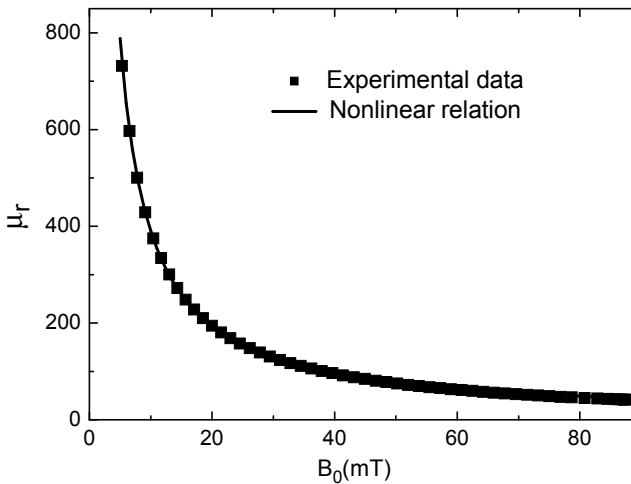

Figure 2: Relative permeability μ_r vs. external magnetic field

3.3   *Numerical results and discussions*

The calculated region of the magnetic field distribution is $800 \times 200 \times 200 \text{mm}^3$ in the FEM simulation. The convergence of FEM is evaluated using various finite element meshes. One has 36000 elements, and the other has 80000 elements. In the examples to follow, the increase in the number of elements does not affect the

shielding efficiency, i.e. maximum difference less than 0.1%. For this reason, the results in this paper are generated from the mesh with 36000 elements. Firstly, the shielding efficiency of single layer enclosure is discussed. The distribution of magnetic field intensity **H** inside and outside the enclosure along the direction of the external magnetic field (i.e. Y axis) is shown in Fig. 3. It can be seen that the values of **H** have a dramatic decrease in the media (42mm<y<45mm) because of the existence of a demagnetizing field due to the magnetization. The values of **H** inside the enclosure (45mm<y<155mm), i.e. the shielded region, lower than the values outside the enclosure (y<42mm or y>158mm), which means some magnetic shielding effect can be achieved with the enclosure. It also can be noticed that the magnetic field intensity inside the enclosure becomes a concavely parabola distribution instead of a constant. The minimum value of **H** exists in the midpoint of the enclosure (see Fig. 3). To make our prediction give some reliable recommendations to the magnetic shield design, the magnetic field induction with shield ($\mathbf{B}_1$) referred to the maximum magnetic field in the enclosure hereinafter.
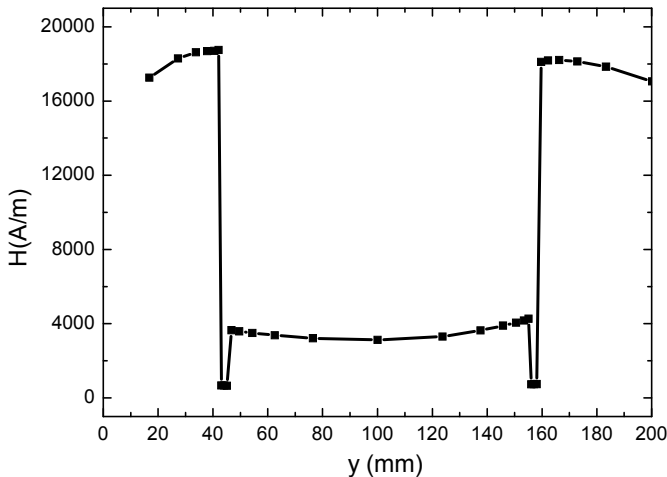

Figure 3: The distribution of the magnetic field intensity **H** along y-direction.

In order to evaluate the reliability of the numerical simulations obtained here on the shielding efficiency of magnetic shielding enclosures, we give some quantitative predictions to compare with experimental data. It can be seen by comparing the second column and the third column in Tab. 1 that the predictions by 3-D finite element calculation with the nonlinear law of magnetization are close to the

measurements. For comparing, the analytical calculation [Hoburg (1996)] and 2-D finite element calculation with the nonlinear law of magnetization are also shown in the Tab. 1. It is shown that results from the analytical calculation or 2-D finite element calculation are far higher than measurements (i.e. the predicted shielding efficiency is low than the actual one), especially 2-D finite element calculation, in which the difference is up to 64%. That is to say, if the shielding enclosure design based on these calculations, some problems such as material waste will arise, and the enclosure is too thick to meet the requirement of saving occupied space. Moreover, it can also be seen that the 3-D finite element result by the linear law of magnetization under 20mT magnetic field (here the average relative permeability μ_r of Fe-Ni alloy 1J79 in the region of measurement is used) is 53.1% higher than the experiment one. As the external magnetic field increases, the predicted results are lower than the experiment ones, i.e. the predicted shielding efficiency is higher than the actual one, which would make the shielding enclosure design cannot meet the shielding requirement.

Now we analyze the effects of permeability, enclosure size and external magnetic field on the shielding efficiency. The shielding factor that is defined in a point as

$$\lambda = \mathbf{B}_0/\mathbf{B}_1 \tag{23}$$

is introduced to describe the shielding efficiency, in which $\mathbf{B}_0$ is the external magnetic field. As $\mathbf{B}_0$ is given, the larger the λ is, the higher the shielding efficiency is. Fig. 4 gives the curves of the magnetic field with shield ($\mathbf{B}_1$) as a function of relative permeability with different thickness (3mm, 5mm, 7mm) subjected to 50mT external magnetic field. It is evident that $\mathbf{B}_1$ decreases with increasing the permeability. And if the permeability is given, $\mathbf{B}_1$ decreases with increasing the thickness of enclosure as shown in Fig. 5. Fig. 6 illustrates the shielding factor of a 3mm enclosure for the applied magnetic field changes from 10mT to 80mT. It is evident that the shielding factor has a remarkable decrease with increasing the magnetic field as nonlinear magnetization is taken into account, while it remains a constant as linear magnetization is considered. That is, the shielding efficiency will vary with surrounding magnetic field, which cannot be captured by the linear law of magnetization.

There are some unavoidable apertures located on walls of the shielding enclosure which would break the magnetic circuit. It is concluded from calculations that the effect of apertures which face to the direction of applied magnetic field on the shielding efficiency is dominate, therefore, we focus on the influence of the size, location and number of apertures in this case on the shielding efficiency. Since the shielding efficiency for circular aperture is the same as the one for square aperture while area is same [Kumar and Venkatesh (2009)], the goal of this paper is to study

Table 1: Comparison of four theoretical models with experimental data (Unit: mT). (The differences are calculated by $(\mathbf{B}_1-\mathbf{B}_e)/\mathbf{B}_e\times100\%$)

Magnetic field without shield $\mathbf{B}_0$	Experimental data $\mathbf{B}_e$	Magnetic field with shield $\mathbf{B}_1$							
		Nonlinear numerical results (3D)	% Difference	Analytical results	% Difference	Nonlinear numerical results (2D)	% Difference	Linear numerical results (3D)	% Difference
20.0	3.2	3.9	23%	4.5	40%	5.3	64%	4.9	53.1%
29.0	6.4	7.8	21%	8.7	36%	10.0	56%	5.7	-10.9%
39.2	13.2	13.9	5%	14.6	10%	16.4	24%	9.7	-26.5%
49.0	20.0	20.5	2.5%	20.9	5%	23.2	16%	11.6	-42%
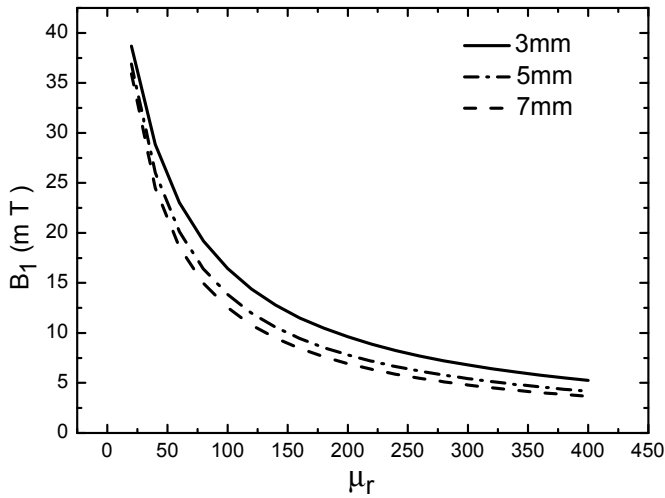
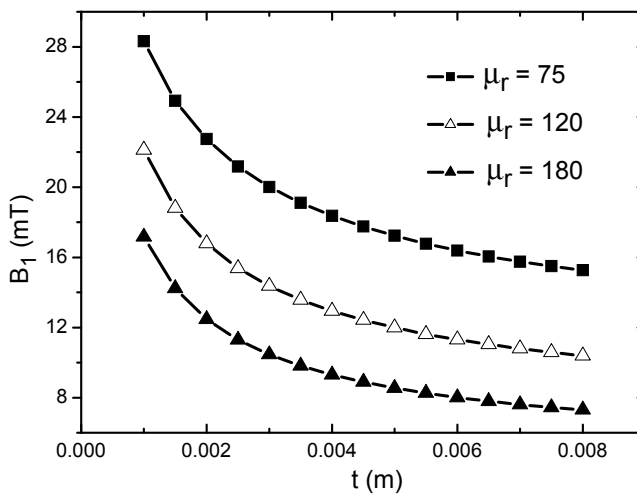Figure 4: Magnetic field with shield $\mathbf{B}_1$ vs. relative permeability μ_r.

Figure 5: Magnetic field with shield $\mathbf{B}_1$ vs. shield thickness t.
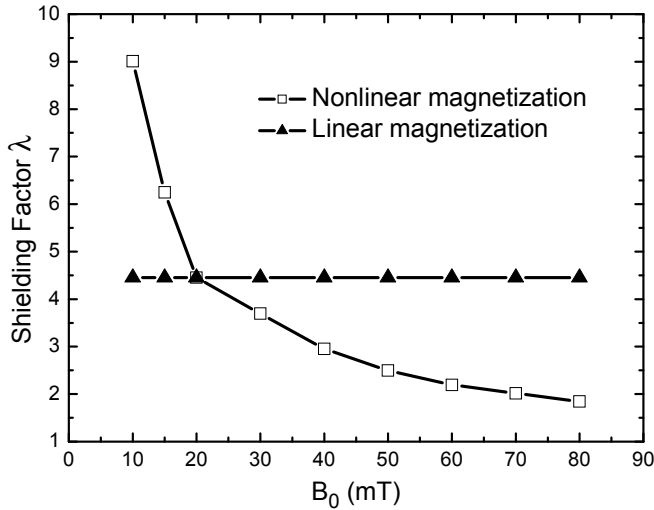
Figure 6: Shielding Factor λ vs. magnetic field without shield $\mathbf{B}_0$.

rectangular apertures. Figure 7 plots the curve of shielding efficiency as a function of the area of an aperture. It can be noticed that shielding factor decreases from 2.5 to 1.8 as the aperture area increases to 0.016m^2. Moreover, as shown in Tab. 2, when an aperture is located in the corner of rectangular enclosure, or in the middle of the short/long edges, or in the middle of enclosure surface, there is only a little difference among them in the shielding factor. Therefore, the aperture area has a remarkable effect on the shielding efficiency, while the location of the aperture has little influence. In addition, it can be seen from Tab. 3 and Tab. 4 that for the area of each aperture is given, shielding degrades significantly as the number of apertures increases (see Tab. 3), while shielding improves slightly with the number of apertures for the area of total aperture is given (see Tab. 4).

For the magnetic shield design in the ITER feeder cubicles, since the cryogenic

Table 2: Influence of aperture locations on shielding effectiveness

	Corner	Middle of short edge	Middle of long edge	Middle of the surface
$B_1(\text{mT})$	22.5	22.7	22.4	23.3
λ	2.22	2.20	2.23	2.15

Table 3: The influence of the aperture number on the shielding efficiency (The area of each aperture is S=0.0004m^2).

Number	B$_1$(mT)	λ
0	21.1362	2.36562
1	21.1756	2.36121
2	21.2050	2.35793
4	21.3603	2.34079
6	21.5225	2.32315
8	21.6246	2.31218
9	21.7565	2.29816

Table 4: The influence of the aperture number on the shielding efficiency (The area of total apertures is S=0.0066m^2).

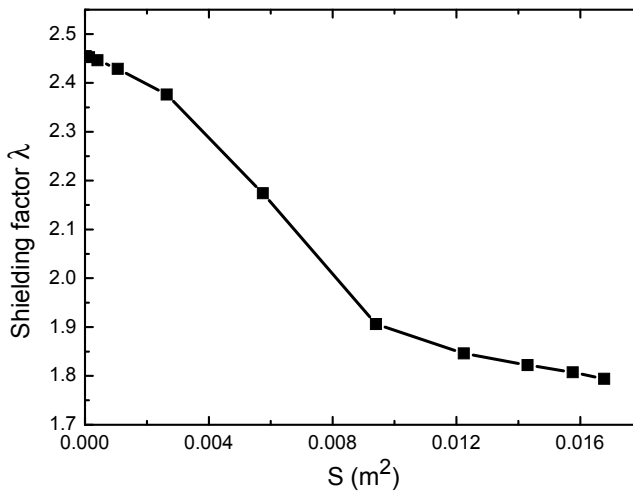| Number	B$_1$(mT)	λ
1	23.632	2.11578
2	23.496	2.12802
4	22.586	2.21376

Figure 7: Shielding Factor λ vs. the area of an aperture.

valves are numerous and densely arranged, the thicknesses for shielding enclosures are limited. In that case, if the single layer enclosure cannot achieve a sufficient shielding effect under the limit, a multilayer design should be considered. The double layer shields are used commonly in applications. Fig. 8 compares the shielding efficiency for two various single layer enclosures and a double layer enclosure. It can be noticed from the figure that two single layer enclosures have similar shielding efficiency for the external magnetic field below 20mT, while the double layer enclosure shows much more shielding efficiency. Moreover, as the external magnetic field above 30mT, the shielding difference between the magnetic field with shield and without shield (i.e. $\Delta \mathbf{B} = \mathbf{B}_0 - \mathbf{B}_1$) by the double layer enclosure has reached 2 times the one by the 3mm single layer enclosure, and is about 1.4 times the one by the 6mm single layer enclosure. That means multilayered shields can provide considerably better magnetic shielding than single-layered shields with the same total thickness.
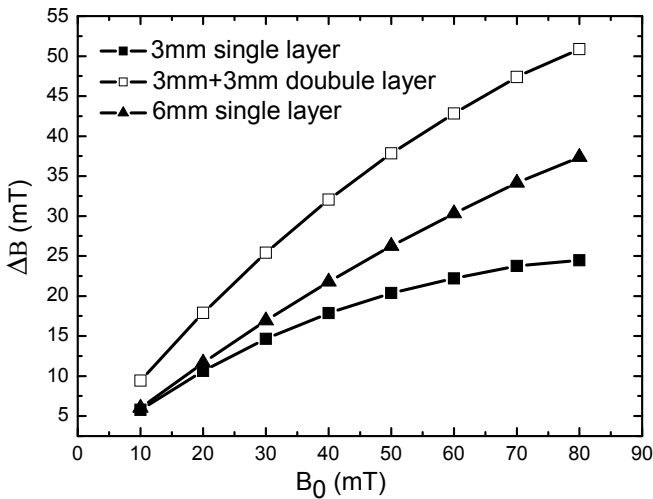

Figure 8: Shielding difference $\Delta \mathbf{B}$ vs. external magnetic field $\mathbf{B}_0$

Then, we analyze the effects of various parameters of materials and configurations on the shielding efficiency. Fig. 9 plots the shielding factor of double layer enclosures with three various thicknesses of insulative layers as a fuction of the external magnetic field. As shown in the figure, the shielding factor decreases with increasing the external magnetic field and increses with the thickness of insulative layer.

Furtherover, the difference of shielding factor among three kinds of double layer enclosures is decreasing with increasing the external magnetic field. When the external magnetic field is greater than 40mT, the effect of thickness of insulative layer does not provide very significant changes in shielding capabilities.
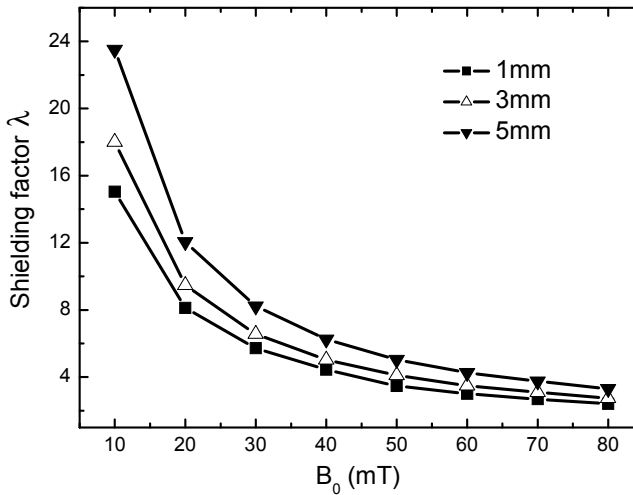

Figure 9: Shielding Factor λ vs. magnetic field before shielding B_0

In addition, different designs for shielding enclosure are investigated. It worth to note from Tab. 5 that shielding performace improves with increasing the thickness of the inner layer and decreasing the thickness of the outer layer for the total shield thickness is given. Therefore, a double layer shield design with a thin outer layer and a thick inner layer is recommended. Moreover, different materials for layers also have an influence on the shielding efficiency. As shown in Tab. 6, double layer shields with a low permeability outer layer and a high permeability inner layer can provide considerably better magnetic shielding.

4   Conclusions

A 3-D theoretical model with the nonlinear law of magnetization for Fe-Ni alloy magnetic shielding enclosures based on FEM is developed. The proposed model can describe the distribution of magnetic field in the shields, and can predict the magnetic shielding efficiency of enclosures, in the presence of excellent agreement

Table 5: Magnetic field $\mathbf{B}_1$ with different thickness of double layer shields ($\mathbf{B}_0$ is 50mT, the thickness of the insulative layer is 1mm).

Thickness t_1 (outer layer)	Thickness t_2 (inner layer)	B_1
4mm	4mm	5.71mT
3mm	5mm	5.0mT
5mm	3mm	6.4mT
2mm	6mm	4.85 mT
6mm	2mm	7.5 mT
1mm	7mm	4.56 mT
7mm	1mm	9.8 mT

Table 6: Magnetic field $\mathbf{B}_1$ with different average relative permeability of double layer shields ($\mathbf{B}_0$ is 50mT, the thickness of the insulative layer is 1mm).

μ_{r1} (outer layer)	μ_{r2} (inner layer)	B_1
80	30	10.3mT
30	80	7.2mT
100	50	7.4mT
50	100	5.6mT
150	100	4.4mT
100	150	3.6mT

with the experimental results. With this model, a step by step analysis of possible magnetic shielding design is presented. The influence of shielding materials, enclosure configurations and apertures on the shielding efficiency is investigated. Furthermore, single or multi- layer designs for shields are also discussed.

Through specific example simulations for the ITER applications, this paper has addressed some conclusions with regard to the magnetic shielding enclosures as follow

(1) The predictions by 3-D finite element calculation with the nonlinear law of magnetization are close to the measurements compared to the ones by the analytical calculation or 2-D finite element calculation. With the linear law of magnetization, the predicted shielding efficiency which is higher than the actual one would make the shield design cannot meet the shielding requirement.

(2) The aperture area has a remarkable effect on the shielding efficiency, while the location of the apertures has little influence. For the area of each aperture is given, shielding degrades significantly as the number of apertures increases,

while shielding improves slightly with the number of apertures for the area of total aperture is given.

(3) Multilayered shields can provide considerably better magnetic shielding than single-layered shields with the same total thickness. And the effect of thickness of insulative layer does not provide very significant changes in shielding capabilities.

(4) As a design alternative, a multilayered shield design with a thin outer layer and a thick inner layer is recommended, and the one with a low permeability outer layer and a high permeability inner layer can provide considerably better magnetic shielding.

References

Bottauscio O., Chiampi M., Manzin A. (2004): Numerical analysis of magnetic shielding efficiency of multilayered screens, *IEEE Transactions on Magnetics*, 40(2), 726–729.

Feng C. and Shen Z. (2005): A hybrid FD-MoM technique for predicting shielding effectiveness of metallic enclosures with apertures, *IEEE Transactions on Electromagnetic Compatibility*, 47(3), 456-462.

Hoburg J. F. (1996): A computaitional methodology and results for quasistatic multilayered magnetic shielding, *IEEE Transactions on Electromagnetic Compatibility,* 38(1), 92-103.

Jiles D. C. (1991): Introduction to Magnetism and Magnetic Materials, New York: Chapman and Hall.

Koroglu S., Sergeant P., Umurkan N. (2010): Comparison of analytical, finite element and neural network methods to study magnetic shielding, *Simulation Modelling Practice and Theory*, 18, 206–216.

Koroglu S., Umurkan N., Kilic O., Attar F. (2009): An approach to the calculation of multilayer magnetic shielding using artificial neural network, *Simulation Modelling Practice and Theory*, 17, 1267–1275.

Kumar T. and Venkatesh C. (2009): Shielding Effectiveness Comparison of Rectangular and Cylindrical Enclosures with Rectangular and Circular Apertures using TLM Modeling, *Applied Electromagnetics Conference (AEMC)*, 1-4.

Omura A., Kotani K., Yasu K., Itoh M. (2006): Analysis of the magnetic distribution within a high-temperature superconductor magnetic shielding cylinder by use of the finite element method, *Journal of Physics and Chemistry of Solids*, 67, 43–46.

Rücker A. W. (1894): On the magnetic shielding of concentric spherical shells, *Phil. Mag.,* 37, 95-130.

Shen Z. (2006): Shielding Effectiveness of Cylindrical Enclosures with Annular Ring Apertures, *17th International Zurich Symposium on Electromagnetic Compatibility*, 38-41.

Shen Z. and Zheng B. (2008): Shielding effectiveness of cylindrical enclosures with rectangular apertures, *Asia-Pacific Sympsoium on Electromagnetic Compatibility & 19th International Zurich Symposium on Electromagnetic Compatibility*, 710-713.

Sumner T. J., Pendlebury J. M. and Smith K. F. (1987): Conventional magnetic shielding, *Journal of Physics D: Applied physics*, 20, 1095-1101.

Umurkan N., Koroglu S., Kilic O. (2010): A neural network based estimation method for magnetic shielding at extremely low frequencies, *Expert Systems with Applications*, 37(4), 3195-3201.

Wulf M. De, Wouters P., Sergeantc P., Dupré L., Hoferlin E., Jacobs S., Harlet P. (2007) Electromagnetic shielding of high-voltage cables, *Journal of Magnetism and Magnetic Materials*, 316, 908-911.

Yenikaya S. and Akman A. (2009): Hybrid MoM/FEM modeling of loaded enclosure with aperture in EMC problems, *International Journal of RF and Microwave Computer-Aided Engineering*, 19(2), 204–210.